Applied Thermal Engineering 31 (2011) 3885–3896

Contents lists available at ScienceDirect

Applied Thermal Engineering

journal homepage: www.elsevier.com/locate/apthermeng

Numerical investigation of burner positioning effects in a multi-burner flameless combustion furnace

B. Danon [a,b,*], E.-S. Cho [a], W. de Jong [a], D.J.E.M. Roekaerts [a,b]

[a] Energy Technology, 3ME Faculty, Delft University of Technology, The Netherlands
[b] Multi-Scale Physics, Faculty of Applied Sciences, Delft University of Technology, The Netherlands

ARTICLE INFO

Article history:
Received 29 May 2011
Accepted 19 July 2011
Available online 26 July 2011

Keywords:
Flameless combustion
Multi-burner furnace
CFD simulation
Burner positioning

ABSTRACT

In this paper results are presented of a numerical study performed for four different burner configurations in a furnace equipped with three pairs of flameless combustion burners firing Dutch natural gas. The simulations have been validated against previously published results of an experimental study [1]. The commercial Computational Fluid Dynamics (CFD) code Fluent 6.3 was used for the calculations. Using the Eddy Dissipation Concept (EDC) model for turbulence–chemistry interaction in combination with the realizable k–ε model for turbulence and a skeletal chemistry mechanism, the main furnace performance was consistently reproduced for all the investigated burner configurations. Moreover, it was found that due to relatively low Reynolds numbers in the cooling air flow in the annulus of the cooling tubes, predictions of the heat extraction rates of these cooling tubes were improved by treating the flow in the cooling tubes as laminar. Furthermore, the applied error tolerance of the ISAT procedure was insufficient for accurate species concentration predictions, however, based on analysis of the main species concentrations in the flue gas, this inaccuracy did not influence the overall predictions.

The most important experimental results have been investigated using the CFD simulations. Firstly, a longer path length from the firing burners to the stack, compared to the path length to the regenerating burners, explained the lower CO emissions in the flue gas in the stack. Secondly, it was found that a recirculation zone between the upper firing burners and the stack in configurations C4 and C5 resulted in a smaller fraction of the flue gases leaving the furnace via the stack compared to the other configurations. Thus, a larger fraction left the furnace via the regenerating burners and this resulted in higher preheat temperatures of the combustion air. Furthermore, more pronounced recirculation zones in configurations C3 and C4 led to higher temperature uniformities in the furnace. Finally, it was confirmed that the jets of the burners in configurations C1 and C3 showed similar merging behavior, leading to similar NO emissions, as observed in the experiments.

1. Introduction

The industrial wish for higher energy efficiency of large-scale furnaces, and its associated fuel savings, has demanded for new combustion technologies, combining heat recirculation from the flue gas with low pollutant emissions. Flameless combustion (also known as flameless oxidation (FLOX) [2], HiTAC [3] or MILD combustion [4]) is such a novel combustion technique. In this technique the combustion air can be highly preheated, without increasing the pollutant emissions, in particular NO_x. The air and fuel are injected at high velocity and spatially separated. Due to this high momentum injection, large quantities of hot flue gases are entrained into the jets before they mix with each other, lowering the oxygen availability in the reaction zone, thus, also lowering the local reaction rates and the peak temperatures. These low peak temperatures reduce the thermal NO emissions [5].

Since the introduction of flameless combustion in the early nineties of the last century, many universities and research departments of industry have made efforts in experimentally investigating this new technology. These studies have been performed on many different scales, from single open flames in jet-in-hot-coflow setups [6,7] to (semi-)industrial scale test furnaces equipped with multiple burners [8–11]. A focus is here on furnaces equipped with multiple flameless combustion burners.

Many of these experimental studies have been complemented with Computational Fluid Dynamics (CFD) simulations. In the

* Corresponding author. Energy Technology, 3ME Faculty, Delft University of Technology, The Netherlands.
E-mail address: b.danon@tudelft.nl (B. Danon).

1359-4311/$ – see front matter © 2011 Elsevier Ltd. All rights reserved.
doi:10.1016/j.applthermaleng.2011.07.036

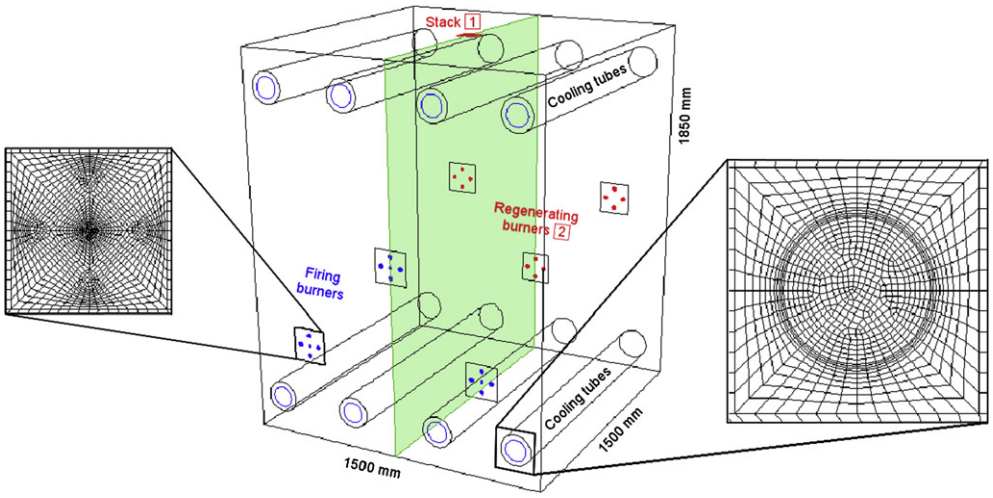

Fig. 1. Furnace sketch, representing burner configuration C5 firing in parallel mode. The boxed numbers 1 and 2 indicate the two sample positions for the flue gas. Sampling point 2 is after the regenerators. The vertical symmetry plane is indicated by the (green) shaded plane. All dimensions are in mm. The two inserts show enlarged front views of the mesh around a burner (left hand side) and a cooling tube (right hand side). The total mesh contains approximately 1.5 million hexahedral cells. (For interpretation of the references to colour in this figure legend, the reader is referred to the web version of this article.)

following the quality of these simulations of furnaces with multiple flameless combustion burners and the choice of physical models in these simulations are discussed.

The 200 kW_th semi-industrial furnace at the Royal Institute of Technology (KTH) has been simulated extensively using the STAR-CD CFD package [12]. Besides the standard $k-\varepsilon$ turbulence model, several combustion models have been investigated, of which the combination of the Eddy Dissipation model and Finite Rate chemistry (ED/FR) turned out to give better results. A two-step chemical mechanism for the combustion of the fuel (LPG, i.e., propane), with CO as an intermediate, was used. Thermal radiation was calculated with the Discrete Transfer method and the absorption coefficient of the gases using the Weighted Sum of Gray Gases (WSGG) model. The cooling tubes were not incorporated in the simulation, but a temperature, based on measured temperatures, was set as a boundary condition. For the validation of the simulations measured heat fluxes, wall temperatures and in-furnace species concentrations were used [13]. The validation results were reasonable, however, the in-furnace temperatures, which this set of models is known to overpredict, were not compared. The three experimentally investigated firing modes, i.e., which combination of burners form a burner pair, were also investigated numerically. The main differences observed in the experiments were reproduced by the simulations. Initially, the analysis of the results was focused on the fundamental properties of flameless combustion. In a later study (firing natural gas) also the observed and reproduced differences between the firing modes were investigated numerically in more detail [14].

In 2004 Hekkens et al. simulated the experiments performed with the 1000 kW_th IFRF furnace firing natural gas using the Fluent CFD package [15,16]. Again, the standard $k-\varepsilon$ turbulence model was used. Three different combustion models were applied; two Probability Density Function (PDF) methods, assuming chemical equilibrium and laminar flamelets, and the ED/FR model. In this last model a two-step chemistry for the combustion of methane was used. Radiation was incorporated using the Discrete Ordinates method and the absorption coefficient was calculated with the domain-based WSGG model. After detailed comparison of the numerical and experimental results, it turned out that the ED/FR model performed best regarding the species concentration predictions inside the furnace. The PDF methods were unable to correctly predict the temperatures inside the furnace, which can be explained by the fact that they assume (too) fast chemistry. However, also the ED/FR model overpredicted the peak temperatures inside the furnace, even though two model constants have been adjusted for flameless combustion purposes using previous IFRF measurements.

The 200 kW_th natural gas fired flameless combustion furnace at the Faculté Polytechnique de Mons has been simulated by Lupant et al. using the Fluent CFD package [10,17,18]. The standard $k-\varepsilon$ turbulence model is applied, with a model constant adjusted for improved prediction of the spreading rate of the jets. Combustion modeling is done using both the PDF method assuming chemical equilibrium and the combined ED/FR model. Again, as in the simulations for the IFRF furnace, two model constants in the ED/FR model were changed in order to improve the results. A one-step

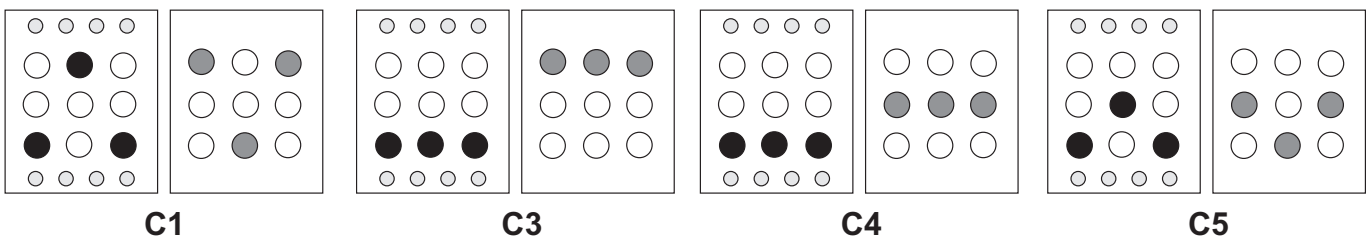

Fig. 2. Overview of simulated burner configurations. The two rectangles represent the two side walls of the furnace with the burner flanges. The large circles represent the burner flanges, if filled black it is occupied by a firing burner, if filled gray it is occupied by a regenerating burner. The black and gray circles switch after a period of 30 s. The small circles denote the position of the cooling tubes.

Table 1
Composition of actual and simulation fuel for Dutch natural gas [26].

Component	DNG	
	Actual	Simulation
	%-mass	%-mass
CH_4	69.97	75.98
C_2H_6	4.63	–
C_3H_8	0.90	–
C_4H_{10}	0.47	–
C_5H_{12}	0.16	–
C_6H_{14}	0.23	–
O_2	0.02	0.02
N_2	21.52	21.87
CO_2	2.10	2.13

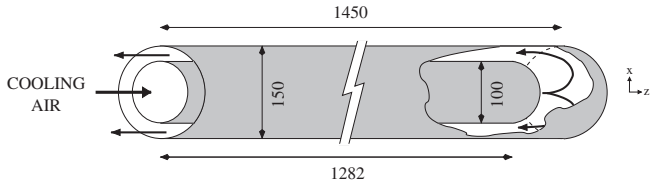

Fig. 3. Schematic representation of a single cooling tube. All dimensions are in mm.

chemistry mechanism has been used for the combustion of methane. Radiative heat transfer is modeled using the Discrete Ordinates method and the WSGG model was used for the calculation of the absorption coefficient. Validation of the simulation is performed by comparison of the numerical results with in-furnace radiative heat flux, temperature and species measurements. Reasonable agreement was achieved for the heat fluxes, however, all simulations overpredicted the temperature inside the furnace. This difference was smaller in the simulation where the model constants in the ED/FR model were adjusted. Although the maximum concentrations of O_2 were predicted rather well, the concentration dropped too fast after its maximum. This indicates that the combustion reactions are too fast, which also explains the prediction of the temperatures being too high. Finally, it is noted that the modification of the model constant in the turbulence model improved the prediction of the delay in the reaction.

Several regenerative reheating furnaces at the NKK steel company firing Low Calorific Value gases were simulated by Ishii et al. using the Fluent CFD package [11,19,20]. Again, the standard $k-\varepsilon$ model for turbulence is used. For the modeling of the combustion the PDF method assuming chemical equilibrium is applied. Radiation is incorporated using the P-1 model and again the WSGG model was used for the absorption coefficient. Besides this standard set of models, a wide variety of models for turbulence, wall functions and PDF shapes were compared [21]. The simulations are validated against in-furnace temperature measurements [11]. The agreement is reasonable outside the combustion zone. Inside the combustion zone the temperatures are fairly overpredicted, as was observed also in the other simulations using a PDF method. After the validation of the simulation, several numerical investigations were performed [19,20].

Generally, it can be concluded that combustion models assuming fast chemistry (e.g. PDF methods assuming chemical equilibrium) are not applicable for the simulation of flameless combustion. Also, a careful choice of the chemical mechanism is important.

At Delft University of Technology (DUT) a 300 kW_th furnace equipped with three pairs of flameless combustion burners, with the unique possibility to vary the positions of the burners in the furnace, has been investigated experimentally [1,22]. In this paper the results of detailed CFD simulations of this furnace are presented. The objective of the simulations was to investigate and explain the observed trends in the furnace performance for the different burner configurations in the furnace.

2. Experimental setup

The furnace is equipped with three pairs of regenerative flameless burners. The burner pairs have a thermal power of 100 kW_th each, thus 300 kW_th in total. The furnace has inner dimensions of 1500 × 1500 × 1850 mm (length × width × height). The insulation consists of three layers of ceramic fire bricks, together 300 mm thick. In total 18 flanges for the burners are divided over two opposite sides of the furnace (nine each). In this way, it is possible to investigate different burner configurations in the furnace. The heat sink is made of eight single ended cooling tubes, four placed above the burners and four beneath, see also Fig. 1 and Section 3.2.

The burners were manufactured by Wärmeprozesstechnik GmbH and are of the REGEMAT CD 200 type. Each burner has four combustion air/flue gas nozzles around a central fuel nozzle, with diameters of 20 mm and 12 mm, respectively. The burners have ceramic honeycomb heat exchangers (regenerators) incorporated. Eighty percent on mass basis of the flue gas is sucked by a fan via the air nozzles over these honeycombs (thus heating them) for regeneration of the heat, while the remaining twenty percent is leaving the furnace via the central stack at the roof. Three burners are firing simultaneously, while the other three burners are regenerating. After a preset time interval of 10–30 s they switch and the firing burners start regenerating, and vice versa. The cycle time (t_{cycle}) is defined as one periodic cycle, i.e., the sum of the firing

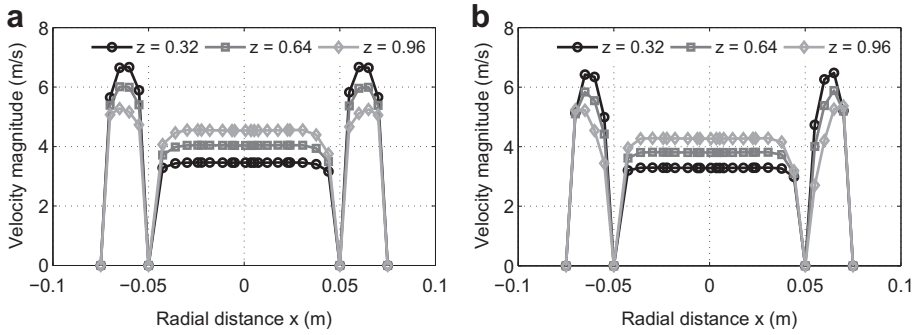

Fig. 4. Predicted velocity magnitude profiles (m/s) in the cooling tube at three axial distances z (m) versus the radial distance x with $x = 0$ at the axis. (a) Realizable $k-\varepsilon$ turbulence model and (b) laminar zone.

Table 2
Heat extraction rate (Q_{tube}) and temperature of the cooling air at the outlet ($T_{coolout}$) of a cooling tube from configuration C1.

Variable	Experiment	Turbulent CFD	Laminar CFD
Q_{tube} (kW)	12.3	18.9	14.6
$T_{coolout}$ (°C)	496	702	550

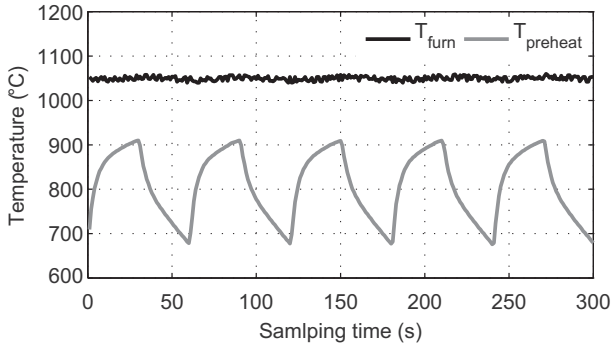

Fig. 5. Furnace temperature (T_{furn}, °C) and preheat temperature of the combustion air ($T_{preheat}$, °C) over a period of 5 entire cycles from the C3 burner configuration experiment.

and regenerating period for one burner. The experimental data with the highest cycle time (60 s) were taken for the present steady RANS simulations, since these experiments are considered to be closest to steady state operation. The data with an excess air ratio (λ) of 1.25 were used for the simulations. Dutch natural gas (DNG) was used as the fuel, which has a net (lower) calorific value of 31.669 MJ/m^3. The furnace operates at atmospheric pressure. Using an NDIR gas analyzer, the NO and CO concentrations in the flue gas from the stack and from the regenerators (boxed numbers 1 and 2 in Fig. 1, respectively) were measured on-line. In the same positions the O_2 concentration was determined on-line paramagnetically for normalization purposes. More details on the experimental setup and results can be found in previous publications [1,22].

Four different burner configurations were investigated numerically. For all of these configurations the firing mode was parallel, indicating that all the firing burners are on one side of the furnace, while all the regenerating burners are on the other side of the furnace. In Fig. 2 the simulated burner configurations are presented.

3. Numerical setup

A three-dimensional mesh of the furnace was generated using Gambit 2.4, see also Fig. 1. The mesh contains approximately 1.5 million hexahedral cells. Exploiting the symmetry of the furnace with respect to its vertical midplane, to reduce the computational time, only half of the furnace is meshed. The cooling tubes are entirely incorporated in the simulations.

The simulations were performed with the commercial code Fluent 6.3.26 [23]. The second order implicit steady solver was used with Green-Gauss cell based interpolation. A SIMPLE algorithm is used for pressure-velocity coupling.

The calculations were performed on a cluster with 4 dual core AMD Opteron 8222 (3.0 GHz) processors with 8 GB DRAM per processor, thus 32 GB in total. The simulations were calculated parallel on all eight nodes.

3.1. Furnace

For turbulence closure the realizable k–ε model was used. This model is shown to give improved results, compared to the standard k–ε model, for the prediction of round jets [24], as is the case in these burners.

For the combustion of the fuel the mechanism of Smooke et al. for the combustion of methane was applied [25]. This so-called skeletal mechanism consists of 16 species (resulting in 16 transport equations to be solved) and incorporates 46 reactions. It is noted here that a mechanism for the reaction of methane only is used. This implies that the Dutch natural gas (DNG) is replaced by a simulation fuel. This simulation fuel contains, as a fuel component, only methane, also replacing the higher hydrocarbons present in DNG, in such way that the heat release per unit mass stays equal. In Table 1 the composition of the actual DNG and its simulation fuel is presented.

The turbulence–chemistry interaction is taken into account by using the Eddy Dissipation Concept (EDC) model [27]. The EDC model has been successfully applied for various turbulent and flameless combustion applications [28,29]. Parente et al. compared results for flameless combustion with different turbulence–chemistry interaction models and chemistry mechanisms [30]. They concluded that the EDC model combined with a skeletal or full chemistry mechanism performed best. Additionally, Stefanidis et al. also compared the EDC model with the combined ED/FR approach [31]. They report that the main disadvantage of the ED/FR model is too fast reaction rates for the oxidization of the fuel. This disadvantage is especially undesired for flameless combustion applications, since in flameless combustion the reaction rates are relatively low. Finally, Kim et al. performed a study on the use of different chemistry mechanisms for the simulation of flameless combustion. The EDC model was used in all the test cases, since it was considered by the authors as a very suitable model for the simulation of flameless combustion [32].

The in situ adaptive tabulation (ISAT) procedure, for the efficient computation of homogeneous reactions in chemically reacting flows, has been applied [33]. The error tolerance of this procedure was stepwise decreased until a value of 10^{-4}. For one case, reported below, the error tolerance was decreased further to a value of 10^{-5}.

Radiative heat transfer is accounted for using the Discrete Ordinates method and the domain-based Weighted Sum of Gray Gases model for the absorption coefficient of the gas mixture. The

Table 3
Comparison of main variables between experiments (EXP) and simulations (CFD) for the four different burner configurations (C1, C3, C4 and C5).

Variable	C1		C3		C4		C5	
	EXP	CFD	EXP	CFD	EXP	CFD	EXP	CFD
T_{furn} (°C)	1036	1121	1051	1113	1074	1142	1052	1128
T_{stack} (°C)	–	1182	–	1192	–	1216	–	1195
Q_{cool} (kW)	99	104	97	101	98	102	90	99
Q_{loss} (kW)	145	110	122	108	141	110	150	110
Q^{*}_{loss} (kW)	137	–	112	–	134	–	144	–
O_2 (%-vol, dry)	3.48	3.22	3.95	4.76	3.22	3.47	3.79	3.43
O_2^{th} (%-vol, dry)	3.66	3.64	5.58	5.56	4.16	4.14	4.03	4.01

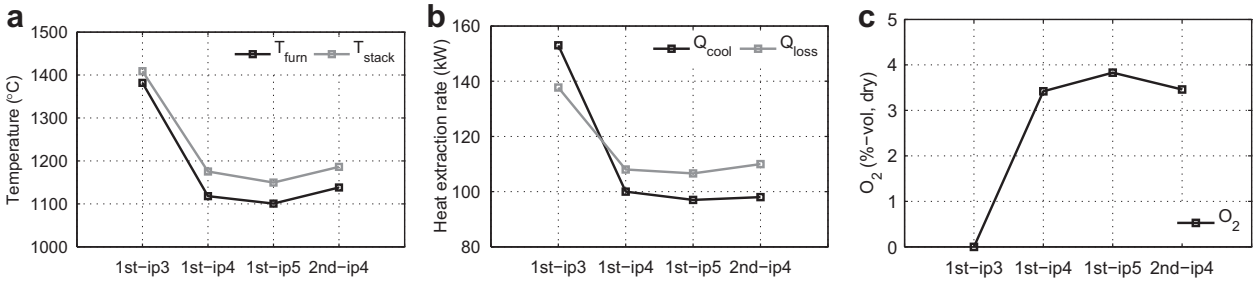

Fig. 6. Main predicted results for configuration C5 parallel versus ISAT error tolerance (IET) and discretization scheme; ip3 = IET of 10^{-3}, ip4 = IET of 10^{-4}, ip5 = IET of 10^{-5}, 1st = first order discretization and 2nd = second order discretization. (a) Furnace temperature (T_{furn}, °C) and flue gas temperature in the stack (T_{stack}, °C). (b) Heat extraction rate of the cooling tubes (Q_{cool}, kW) and other heat losses (Q_{cool}, kW). (c) Oxygen concentration in the flue gas from the stack (%-vol, dry).

mean beam length was based on the dimensions of the furnace since the flue gas composition inside the furnace is reasonably uniform and with this approach improved predictions of the radiation fluxes between the walls and cooling tubes are expected. The emissivity of steel was set to 0.8 and that of the firebrick insulation to 0.68.

The density of the mixture is calculated by the multi-component ideal gas law using the low Mach number approximation $p = p_{ref}$. The molecular viscosity and thermal conductivity of the gas mixture are taken constant at 1.72×10^{-5} kg/ms and 0.0241 W/mK, respectively. The mass diffusivity is calculated by Fick's law with a constant and identical mass diffusion coefficient of 2.88×10^{-5} m^2/s for all species. Finally, the heat capacities are determined per species with a temperature dependent piece-wise polynomial provided by Fluent, and for the mixture with the mixing law.

The heat losses through the walls were incorporated by calculating the convective and radiative heat flux to the environment. For a realistic value of the effective thermal conductivity of the walls, the predicted wall temperatures were compared with the experimental values.

In previous studies this set of models proved to be suitable for the simulation of flameless combustion in furnace environments [34,14]. Additionally, De et al. performed a detailed comparison study of these and comparable models for experimental results of a jet-in-hot-coflow setup, which emulates flameless combustion [35]. Overall, the set of models was well capable of predicting flameless combustion. Moreover, it was shown that the realizable k–ε performed better than other two-equation turbulence models. Also, the use of the above-mentioned constant values for the viscosity and the species mass diffusivities showed no significant differences with simulations with a temperature dependent viscosity or using multi-component diffusion. The largest difference, compared to the experiments, was that the ignition was predicted to occur too early. Finally, a limitation of the use of the EDC model with a skeletal chemistry mechanism was demonstrated for flows with low turbulence Reynolds numbers. In the present furnace the Reynolds numbers were verified to be higher than the Reynolds numbers where these limitations become apparent.

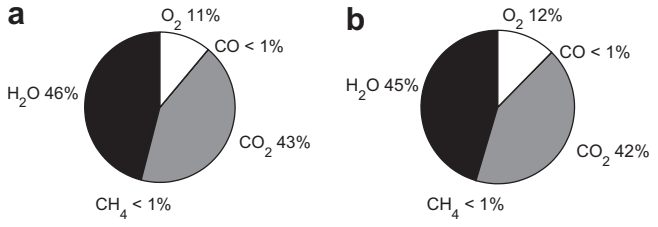

Fig. 7. Main species mass fractions (−) in the flue gas in the stack with burner configuration C5 for (a) IET = 10^{-4} and (b) IET = 10^{-5}.

3.2. Cooling tubes

In preliminary simulations of the furnace the heat extraction rate of the cooling tubes was fairly overpredicted. In order to investigate this difference a separate simulation was performed on a single cooling tube. The mesh of this single cooling tube is kept exactly the same as the mesh of a cooling tube in the mesh of the furnace. As a boundary condition the furnace temperature was set on the outer tube in this separate simulation.

Each cooling tube consists of two concentric annular tubes. Air was used as the cooling medium and enters the inner tube, turns at the end and flows back through the annulus between the inner and outer tubes. This setup was chosen to minimize the temperature gradients along the length of the outer tube, thus, creating an as uniform as possible heat extraction distribution. The inner tube has an internal diameter of 100 mm and penetrates 1282 mm into the outer tube, which in turn penetrates 1450 mm into the furnace and has a inner diameter of 150 mm. In Fig. 3 a schematic representation of a single cooling tube is presented.

In order to characterize the flow regime inside the cooling tube the Reynolds number was calculated. The Reynolds number (Re) is defined in Equation (1).

$$Re = \frac{\rho u d_h}{\mu} \tag{1}$$

where ρ is the mean density (kg/m^3), u the mean velocity magnitude (m/s), d_h the hydraulic diameter (m) and μ the molecular viscosity (kg/ms). The hydraulic diameter d_h is 0.1 m and 0.05 m for the inner tube and the annulus, respectively. The Reynolds number

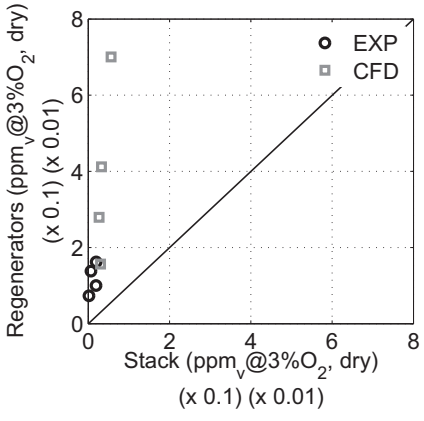

Fig. 8. Comparison of experimental values for CO concentration (0.1 × ppm$_v$ @3%O$_2$, dry, EXP) and predicted values from the simulations (0.01 × ppm$_v$ @3%O$_2$, dry, CFD) in the flue gas from the stack and from the regenerators for all four burner configurations firing in parallel mode.

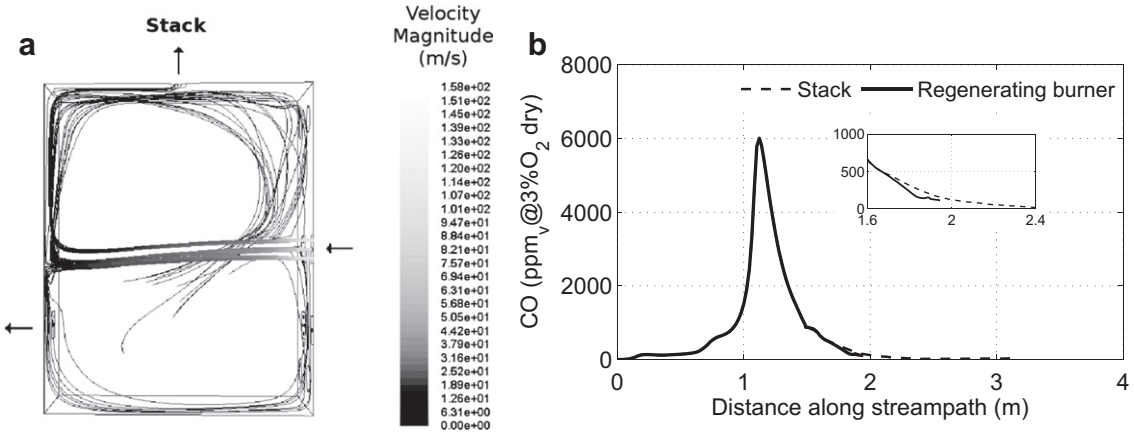

Fig. 9. (a) Sideview of the furnace showing the pathlines from the nozzles of a firing burner in configuration C5. Pathlines are colored by the velocity magnitude (m/s). (b) CO concentration (ppm_v @3%O_2, dry) versus distance along the paths from the firing burner to the opposing regenerating burner (solid line) and to the stack (dashed line). Results from CFD simulations.

of the flow in the inner tube and annulus are around 20,000 and 10,000, respectively. These values indicate that the flow in the inner tube is turbulent, however, in the annulus it is in the range of Reynolds numbers that indicate the transition regime between laminar and turbulent flow.

In order to further investigate the flow regime in the annulus, the predicted velocity magnitude profiles, using the turbulence model, in the cooling tube at three axial positions (z) are presented in Fig. 4(a). Indeed, the velocity profile in the inner tube has the shape typical for turbulent pipe flow. However, the velocity profile in the annulus tend to a parabolic form, which indicates laminar flow.

In a subsequent simulation the entire cooling tube has been treated as a laminar zone. In Table 2 the numerical results for the single cooling tube (with boundary condition values taken from the C1 configuration experiment), treating the flow in the cooling tube either as turbulent or as laminar, are compared with the experimental values. It is observed that the predictions for both the total heat extraction rate (Q_{tube}) and for the temperature of the cooling air at the outlet ($T_{coolout}$) were closer to the experimental values when the cooling tubes were treated as laminar. This can be explained by the flow in the annulus to rather resemble laminar flow behavior and thus creating a sort of thermal resistance, limiting the total heat extraction rate of the cooling tube. In Fig. 4(b) the velocity profiles using the laminar model are presented. It is observed that the velocity profiles in the annulus are more pronounced parabolic.

To conclude, in the furnace simulations, the flow in the cooling tubes is treated separately from the rest of the furnace and as laminar flow. The flow within the furnace itself is still treated as turbulent flow.

3.3. Data comparison

For comparison of the transient experimental data (due to the switching of the burners) and the steady state numerical results, averaging is required. In Fig. 5 the furnace temperature, characterized by a thermocouple in the furnace side wall, and the preheat temperature of the combustion air in one burner are presented over a period of 5 entire cycles. These data are from the C3 burner configuration experiment.

It is noted that the transient behavior is well represented in the preheat temperature, while the furnace temperature is not showing any correlation with the cycle time. Actually, all the measurements used as boundary conditions or for validation of the simulations (wall temperatures, heat extraction rates of the cooling tubes, composition of the flue gas) show similar steady signals.

The preheat temperature of the combustion air is also used as a boundary condition of the simulations, since the regenerators are not incorporated in the simulations. Therefore, the data of the preheat temperature of an entire firing period is averaged and set as the boundary condition.

Furthermore, in order to have a similar spatial heat distribution in the simulations as in the experiments, two separate steady state simulations were performed for each configuration. For both parts of an entire cycle a steady simulation was performed, i.e., one simulation with one set of burners firing and one simulation with the other set of burners firing was performed, see also Fig. 2. For the final comparison of the experimental and numerical results, the results of these two simulations were averaged.

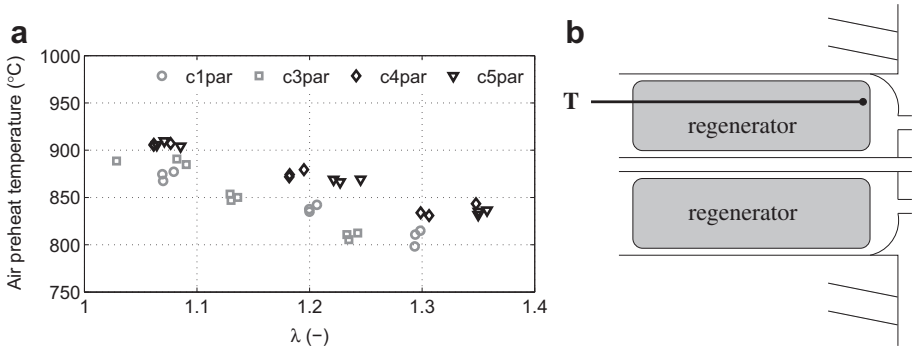

Fig. 10. (a) Experimental values of the combustion air preheat temperatures (°C) for all configurations, parallel firing mode, all values of λ and cycle time [1]. (b) Position of thermocouple in regenerators.

4. Results and discussion

4.1. Validation

In Table 3 the main results of the experiments are compared with the numerical results for all the configurations. It is noted here that all the four configurations are simulated with the exact same set of physical models and settings, as described above.

The furnace temperature is overpredicted in the simulations with around 70° C, however, these differences are considered to be acceptable.

The heat extraction by the cooling tubes (Q_{cool}) is predicted reasonably accurately. The predicted values are slightly higher for all configurations, but the values are close. The other heat losses (Q_{loss}), mainly through the walls, are underpredicted in the simulations. This is partly due to the calculation method of this value in the experiments. In the analysis of the experimental results, the heat flux through the stack is calculated assuming that the flue gas leaving the furnace via the stack is at a temperature equal to the furnace temperature. However, comparing the furnace temperature (T_{furn}) and the flue gas temperature in the stack (T_{stack}) in the simulations, the latter is consistently higher. This indicates that by taking the furnace temperature as the stack flue gas temperature, the experimental heat flux through the stack is underestimated. The values for the experimental heat losses calculated with the predicted temperature of the gas in the stack (Q^*_{loss}) show that this error explains only part of the difference.

Finally, the oxygen concentration (O_2) in the flue gas is considered. In Table 3 the measured and predicted values of the O_2 concentration in the flue gas from the stack are presented. Additionally, the theoretical value (O_2^{th}) calculated from the measured flows of comburants for complete combustion, both using the actual fuel (DNG) and using the simulation fuel (only containing CH_4 as a hydrocarbon, see above), are reported. In the first place, the measured values are compared with the theoretical values for the experiments. All the measured O_2 values are lower than the theoretical values. These differences are, besides the error in the measurement of the oxygen concentration itself, due to errors in the measurement of the comburant mass flows. Secondly, comparing the theoretical values for the actual fuel (DNG) and the simulation fuel, it is noted that they are very similar. Finally, comparing the predicted values in the simulations with the theoretical values for the simulation fuel, it is noted that the predicted values are systematically lower. This is due to the integration of the chemistry in the simulations. As stated before, the ISAT procedure was used for shorter computational times. Gordon et al. investigated the maximal value for the ISAT error tolerance (IET) for several mechanisms [36], concluding a maximal value of 10^{-6} for the Smooke mechanism is required. Due to too long computational times, this value was not supportable for the current mesh in combination with the current cluster.

To verify the impact of the error due to this deficiency, one case (configuration C5 with the black burners firing, see Fig. 2) was run with IET 10^{-5}. In Fig. 6 the main results, as presented in Table 3, are plotted for the simulations with the different values of the IET. It is noted that a large difference in the main results is observed between the simulations with IET 10^{-3} and 10^{-4}. In case of IET 10^{-5} the results do improve, however, relatively marginally. It is concluded here, that these simulations would improve by additional calculation with IET 10^{-5}, however, considering the time investment versus the expected improvement, this was not performed.

Additionally, in Fig. 6, the results of the simulation with IET 10^{-4} with both first order and second order discretization schemes are compared. It is noted that the differences in main results between these two simulations are marginal.

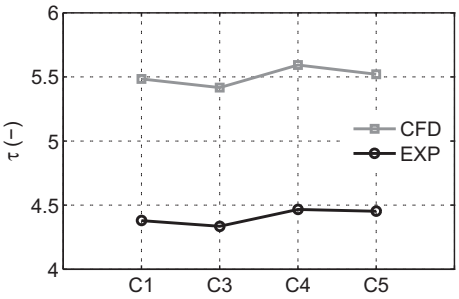

Fig. 11. Comparison of the maximum value of τ (–) at the hot side of the regenerators in the experiments (EXP) and the predicted τ (–) of the flue gas entering the regenerating burners (CFD).

Finally, in Fig. 7 the mass fractions of the main species in the flue gas in the stack are compared for the simulations of configuration C5 with IET 10^{-4} and 10^{-5}. It is noted that in the simulation with IET 10^{-4} lower O_2 concentrations and higher CO_2 and H_2O concentrations are predicted. In the case of IET 10^{-5} the O_2 content is slightly higher and the CO_2 and H_2O contents are lower. Thus, by decreasing the IET the oxygen concentration is tending toward the experimental and theoretical values. For both cases, the concentrations of CO and CH_4 are very low; they are in the order of 10 and 10^{-4} ppm, respectively. It can be concluded that in the simulation with the higher value of IET (10^{-4}) the combustion is complete, i.e., there is hardly any CO and CH_4 left in the flue gas. Therefore, no large errors in the total heat distribution in the furnace due to integration errors are to be expected.

Although no in-furnace measurements were performed for a detailed validation, the consistency of the predictions for all the four investigated configurations confirmed the suitability of the set of physical models for a numerical investigation of this furnace.

4.2. Carbon monoxide emissions

In Fig. 8 the concentrations of CO in the flue gas from the stack and from the regenerators are presented for the experiments and the simulations. For these two flue gas sampling locations, see the boxed numbers in Fig. 1.

All the predicted values of the CO concentration are much higher than the measured values. This is a deficiency of the used chemistry mechanism and was also mentioned as such by the developers of the mechanism [25]. Additionally, in the simulations the CO concentrations in the flue gas from the regenerators are taken before the regenerators (at the hot side), whereas in the experiments this CO concentration is measured after the regenerators (at the cold side). Thus, part of the excess CO observed in the numerical results would have been converted to CO_2 in the regenerators if simulated.

However, the trend in the difference between the values in the flue gas from the stack and from the regenerators is reproduced correctly; in the stack flue gas, relatively smaller amounts of CO are predicted, whereas in the regenerator flue gas larger amounts of CO are predicted.

The difference in the CO concentrations in the two exits is related to the path length of the mean flow to these exits. In Fig. 9(a) the pathlines along the streamlines of the mean velocity

Table 4
Measured mass percentage (%-mass) of flue gas leaving the furnace via the stack.

	C1	C3	C4	C5
Mass percentage stack (%-mass)	27.3	31.2	22.1	22.1

(taken from the CFD simulations) of the gases flowing from the middle firing burner in configuration C5, to the opposing regenerating burners and to the stack are presented. The burners and the stack are indicated by the arrows. It is observed that the pathlines to the stack are longer than those to the regenerating burner. Also, it is noted that part of the gases not immediately leaves the furnace, but is recirculated to the root of the comburants jet.

Based on the observed pathlines from CFD, the approximate path lengths of the mean flow were calculated exploiting only straight lines and right angles. The recirculating gases were not included in this calculation since they join the jet again at its root. Furthermore, it can be assumed that the gases that immediately leave the furnace, either via a regenerating burner or via the stack, account for the largest part of the observed CO concentrations.

The path lengths between all firing burners and all regenerating burners were calculated and subsequently averaged. The same was done for the path lengths between the firing burners and the stack. The averaged path lengths from the firing burners to the regenerating burners and to the stack are approximately 2.0 m and 3.0 m, respectively. For the firing burner in Fig. 9(a) these path lengths were converted to residence times by division with the local velocity. The residence time of the gases from this burner to the regenerating burner was 0.2 s. From the firing burner to the stack the residence time was 0.5 s. Again, these values include the direct paths only, excluding recirculation.

In Fig. 9(b) the CO concentration along the considered paths from the firing burner to the opposing regenerating burner and to the stack are presented from the simulations. The initial 1.5 m is identical for both paths, since in both cases the gases cross the furnace width first. The peak in CO concentration, which can be regarded as the center of the combustion zone, is at approximately 1.2 m from the burner nozzles. After this point, the CO concentration decreases steadily. It is observed that the CO in the gases to the regenerating burner is not fully converted before reaching the exit point. On the other hand, in the gases traveling toward the stack, the CO concentration further decreases (see insert with enlargement in Fig. 9(b)).

Thus, it is concluded that the flue gas leaving the furnace via the stack had a long enough residence time (due to its longer path length) to have most of the CO converted to CO_2.

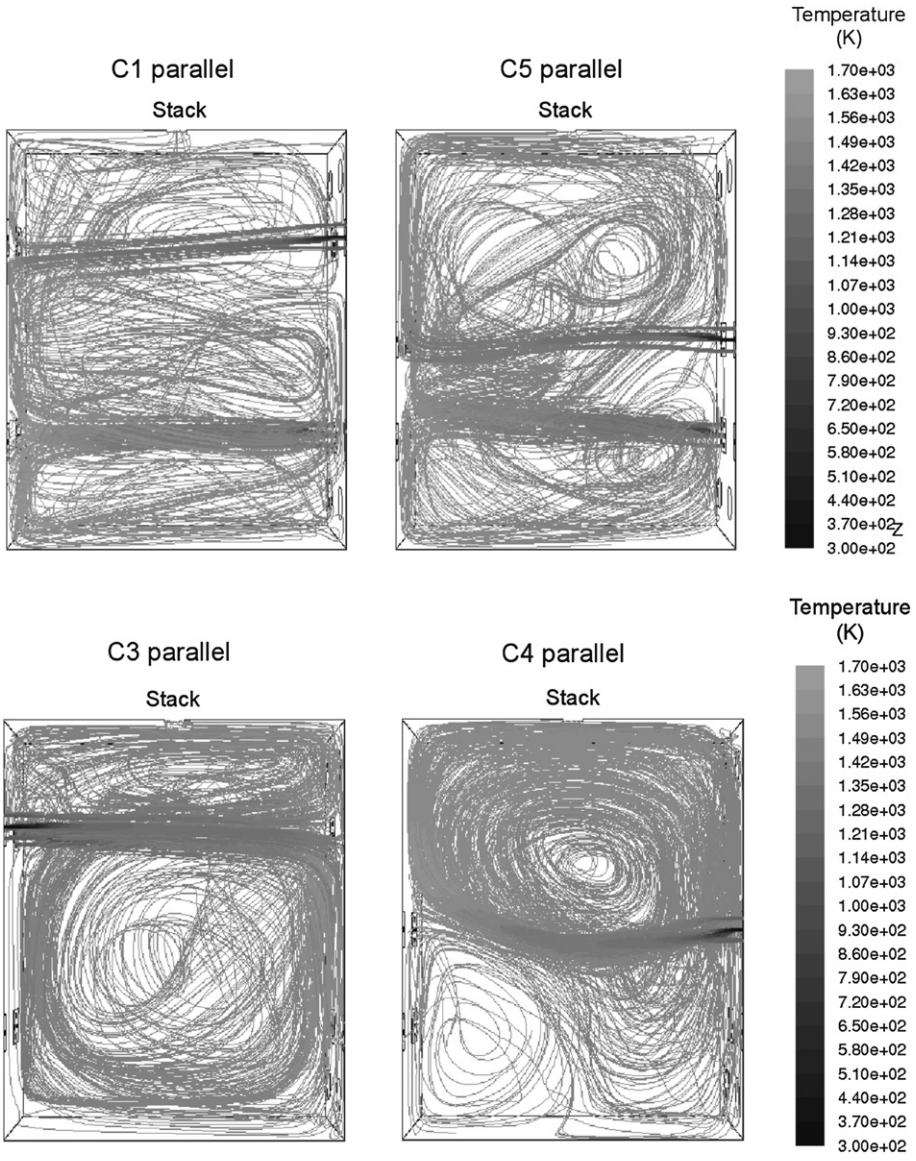

Fig. 12. Pathlines from all grid cells of the firing burner inlets of all configurations colored by the local temperature (K) viewed toward the vertical midplane of the furnace.

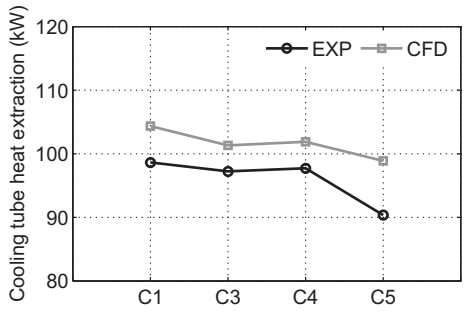

Fig. 13. Cooling tube heat extraction rates (kW) comparison for the experiments (EXP) and simulations (CFD).

4.3. Combustion air preheat temperature

In the experiments a difference in the preheat temperature of the combustion air was observed for the different burner configurations. In Fig. 10 the experimental values of the preheat temperature of the combustion air are presented. It was observed that the preheat temperatures for the C4 and C5 configurations are higher than those for configurations C1 and C3.

In Fig. 11 the maximum value of the normalized temperature (τ) at the hot side of the regenerator in the experiments is compared with the predicted flue gas temperature entering the regenerating burners. The normalized temperature τ is defined in Equation (2).

$$\tau = \frac{T}{T_{\text{ref}}} \tag{2}$$

where T is the temperature (K) and T_{ref} the reference temperature (273.15 K).

The numerical values are higher than the experimental values. This is due to two reasons. In the first place, the thermocouples inserted in the regenerators only penetrate until the end of the regenerators, while in the simulations the flue gas temperature is taken at the nozzle, see also Fig. 10(b). In the second place, the measured temperatures will be slightly lower than the actual gas temperatures due to radiative heat losses of the thermocouples. The reported experimental measurements were not corrected for these radiative losses.

However, in both the experiments and the simulations the values of τ are higher for configurations C4 and C5. This is explained by the amount of flue gas leaving the furnace via the stack. In Table 4 the experimental values of the mass percentage of flue gas leaving the furnace via the stack is presented for the four configurations. It is noted here that the mass percentage of flue gas to the stack is set as a boundary condition in the simulations.

It is observed that for both C1 and C3 relatively larger percentages of the flue gases leave the furnace via the stack. This is

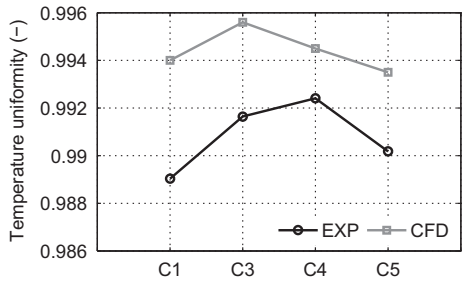

Fig. 14. Temperature uniformity (−) comparison for experiments (EXP) and simulations (CFD).

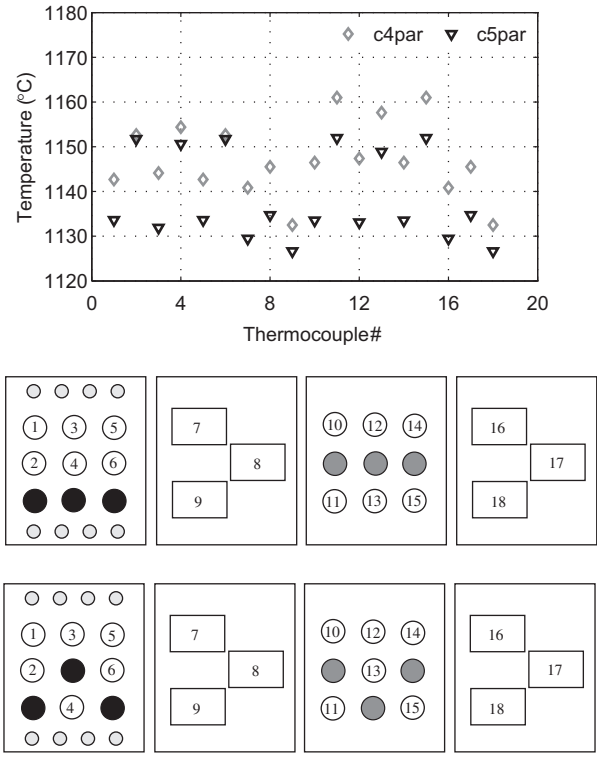

Fig. 15. Predicted temperatures (K) for all thermocouples in burner configurations C4 and C5. The four rectangles represent the four side walls of the furnace with the numbers indicating the positions of the thermocouples.

due to the fact that in these configurations the three higher burners are positioned in the upper level, whereas in C4 and C5 they are positioned in the middle level, see also Fig. 2.

In Fig. 12 pathlines along the streamlines of the mean velocity are presented from all grid cells of the firing burner inlets of all the configurations, colored by the local temperature. It is observed that in configuration C4 and C5, as expected, less of these pathlines leave the furnace via the stack in the roof. This is due to an additional recirculation zone above the firing burners compared to configuration C1 and C3.

It is concluded that in configurations C1 and C3, due to the firing burners positioned closer to the stack and the absence of a recirculation zone between these firing burners and the stack, significantly more flue gas leaves the furnace via the stack and relatively less hot flue gas is available for regeneration, leading to lower preheat temperatures of the combustion air.

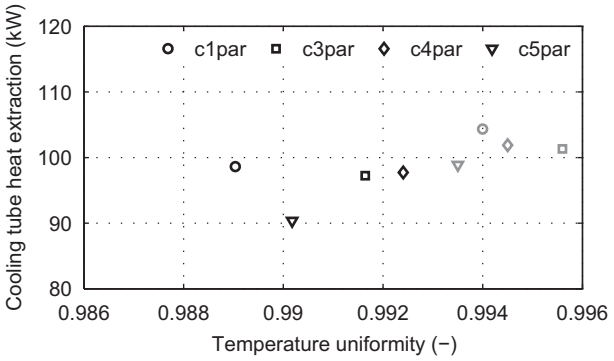

Fig. 16. Cooling tube heat extraction rate (kW) versus temperature uniformity (−) for all burner configurations in parallel firing mode. Black symbols are the experimental values, gray symbols represent the numerical values.

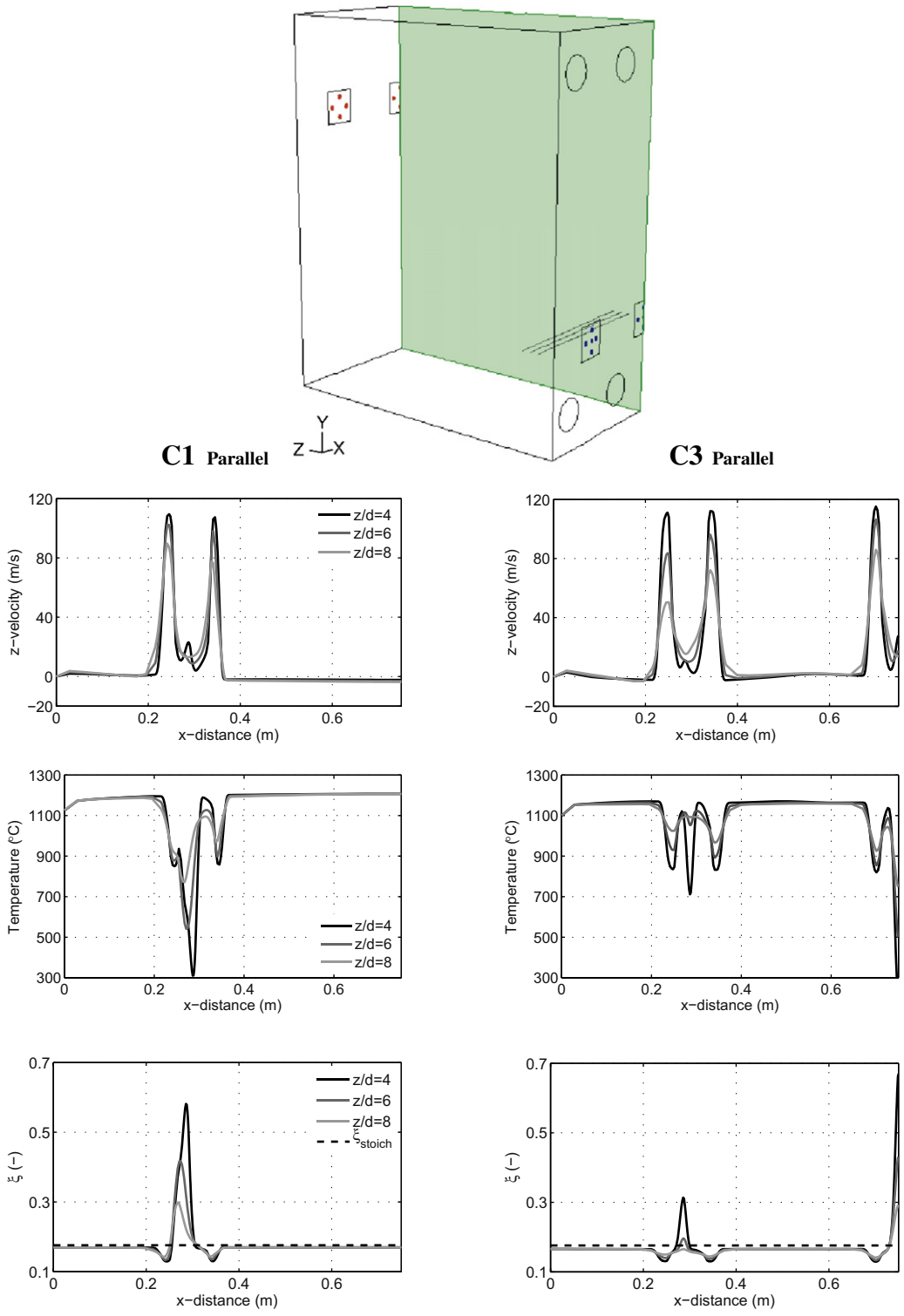

Fig. 17. Development of the velocity in the z -direction (m/s), temperature (°C) and mixture fraction (ξ, –) for the lower burners in configurations C1 and C3 parallel. The data are plotted over the three gray lines depicted in the sketch of the numerical domain of configuration C3. The (green) shaded plane is the vertical symmetry plane. (For interpretation of the references to colour in this figure legend, the reader is referred to the web version of this article.)

4.4. Cooling tube heat extraction

In Fig. 13 the experimental and numerical values of the cooling tube heat extraction rate of the four configurations are compared. The predicted values are slightly higher than the experimental. However, the trend between the different cases is well captured by the simulations.

The cooling tube heat extraction is directly related to the total mass flow of cooling air to the cooling tubes. In the total mass flow of cooling air the same trend is observed as in Fig. 13. Since the

measured total cooling air mass flows are set as boundary conditions in the simulations, the trends in the total cooling tube heat extraction rates are also reproduced in the simulations.

4.5. Temperature uniformity

In Fig. 14 the experimental and numerical values of the temperature uniformity of the four configurations are compared. The temperature uniformity (T_u) is defined as in the following equation.

$$T_u = 1 - \sqrt{\frac{1}{N}\sum_{i=1}^{N}\left(\frac{(T_i - \overline{T})}{\overline{T}}\right)^2} \quad (3)$$

where N is the total number of temperature measurement positions, T_i is the temperature in the ith position and $\overline{T}$ is the mean of all the temperature measurements. The value of the T_u is between 0 and 1, where the value 1 indicates a perfectly uniform furnace.

The trend in the temperature uniformities agrees well between the experiments and simulations. Especially, the observation that configurations C3 and C4 achieve higher temperature uniformities, compared to configurations C1 and C5, is reproduced. However, there is an opposing trend in the temperature uniformities of C3 versus C4 and C1 versus C5.

In Fig. 15 the predicted values for the wall temperatures are presented for burner configuration C4 and C5. The exact positions of the thermocouples are denoted in the drawings of the four side walls of the furnace.

It can be observed, comparing the thermocouples in the highest level (numbers 1, 3 and 5) with those in the middle or lower level (numbers 2, 4 and 6), that the difference in the temperature is larger for configuration C5, which results in a lower temperature uniformity. Actually, in configuration C4, thermocouples 1, 3 and 5 have relatively higher values. This is due to the fact that a stronger recirculation zone in this configuration results in lower temperatures in the upper zone of the furnace, see also Fig. 12. This also explains the lower temperature uniformity in configuration C1, where the least pronounced recirculation zones can be identified. For the values of the thermocouples in the opposite wall (numbers 10 to 15) the same behavior can be observed.

4.6. Temperature uniformity versus cooling tube heat extraction

In the experimental results, a linear correlation was observed between the cooling tube heat extraction and temperature uniformity [1]. In Fig. 16 these values are plotted for both the experiments and the simulations. It is observed that the decreasing trend in the cooling tube heat extraction rate with increasing value of the temperature uniformity is not reproduced. Due to the choice of experiments simulated it is not possible to either confirm or contradict the observations of the experimental results. In order to be able to do this, additional simulations of cases exploiting more variation in the values of the cooling tube heat extraction and the temperature uniformity are required. Due to time limitations, these additional simulations are currently not performed.

4.7. Point of confluence

In a previous study on a comparable furnace [14] the point of confluence of the comburant jets was indicated as an important factor for the NO formation. In this study the NO emissions were similar for all configurations and operating conditions [1]. To verify whether the jets show similar merging behavior in this furnace the firing burners in the lowest level of configurations C1 and C3 are compared.

In Fig. 17 the velocity in the (axial) z -direction, the temperature and the mixture fraction are plotted on lines at three distances from the nozzles of these burners. The distance from the burner nozzles z is normalized by the diameter of the air nozzles d (0.02 m). The fuel nozzles are positioned at $x = 0.295$ m and 0.75 m and are surrounded by two high momentum air nozzles. The mixture fraction was calculated by applying Bilger's formula [37].

The point of confluence is defined as the point where the low-momentum jet is absorbed by the high momentum jet(s) [38]. The further the point of confluence from the nozzles, the more internal flue gas recirculation is present before the fuel and oxidizer jets merge and lower NO emissions are expected.

For the burner at $x = 0.295$ m no clear differences can be observed between configuration C3 and C1, both seem to have a point of confluence at $z/d = 6$. The burner at $x = 0.75$ m has a point of confluence at $z/d = 8$ in both configurations (only configuration C3 is shown in Fig. 17, but the burner of configuration C1 showed the same value). Concluding, it is confirmed that the jets of the burners in configurations C1 and C3 show similar merging behavior, which is in agreement with the proposed explanation for the similar NO concentrations in their flue gases. Also, no distinct differences in the maximum temperatures could be identified between the two configurations. Finally, it can be expected that the middle burner (at $x = 0.75$ m) produces less NO than the two outer burners.

5. Conclusions

A numerical study has been performed for four different burner configurations in a furnace equipped with three pairs of flameless combustion burners. A carefully selected set of physical models proved to be adequate to reproduce the main results observed in the furnace experiments. The simulations have been validated against the main results of the furnace experiments and by consistently capturing the trends in these results for the different burner configurations. Moreover, it was found that due to relatively low Reynolds numbers in the cooling air flow in the annulus of the cooling tubes, predictions of the heat extraction rates of these cooling tubes were improved by treating the flow in the cooling tubes as laminar. Furthermore, the applied error tolerance of the ISAT procedure was shown to be insufficient for accurate species concentration predictions, however, based on analysis of the main species concentrations in the flue gas, this inaccuracy did not influence the overall predictions.

The most important experimental results have been investigated using the simulations. In the first place, a longer path length from the firing burners to the stack, compared to the path length to the regenerating burners, explained the lower CO emissions in the flue gas in the stack. Secondly, it was found that a recirculation zone between the upper firing burners and the stack in configurations C4 and C5 resulted in a smaller fraction of the flue gases leaving the furnace via the stack compared to the other configurations. Thus, a larger fraction left the furnace via the regenerating burners and this resulted in higher preheat temperatures of the combustion air. Furthermore, the total cooling tube heat extraction was directly related to the total amount of cooling air. In the fourth place, more pronounced recirculation zones in configurations C3 and C4 led to higher temperature uniformities in the furnace. Finally, it was confirmed that the jets of the burners in configurations C1 and C3 showed similar merging behavior, leading to similar NO emissions, as have indeed been observed in the experiments.

It can be concluded that by the numerical study more insight is attained regarding the effects of burner positioning in a multi-burner flameless combustion furnace. In the future, the simulations can be improved by further decreasing the error tolerance of

the ISAT procedure. Also, in order to verify the observation in the experiments of a decreasing cooling tube heat extraction with increasing temperature uniformity, additional simulations are required.

Acknowledgements

This project has been financially supported by the Dutch Technology Foundation (STW) and the Dutch Flame Foundation (NVV).

References

[1] B. Danon, E.S. Cho, W. de Jong, D. Roekaerts, Parametric optimization study of a multi-burner flameless combustion furnace, Appl. Therm. Eng. 31 (2011) 3000–3008.
[2] J. Wünning, J. Wünning, Flameless oxidation to reduce thermal NO-formation, Prog. Energy Combust. Sci. 23 (1997) 81–94.
[3] H. Tsuji, A. Gupta, T. Hasegawa, M. Katsuki, K. Kishimoto, M. Morita, High Temperature Air Combustion: from Energy Conservation to Pollution Reduction. CRC Press, 2003.
[4] A. Cavaliere, M. De Joannon, Mild combustion, Prog. Energy Combust. Sci. 30 (2004) 329–366.
[5] J. Miller, C. Bowman, Mechanism and modeling of nitrogen chemistry in combustion, Prog. Energy Combust. Sci. 15 (1989) 287–338.
[6] P. Medwell, P. Kalt, B. Dally, Simultaneous imaging of OH, formaldehyde, and temperature of turbulent nonpremixed jet flames in a heated and diluted coflow, Combust. Flame 148 (2007) 48–61.
[7] E. Oldenhof, M. Tummers, E. van Veen, D. Roekaerts, Ignition kernel formation and lift-off behaviour of jet-in-hot-coflow flames, Combust. Flame 157 (6) (2010) 1167–1178.
[8] N. Rafidi, W. Blasiak, Heat transfer characteristics of HiTAC heating furnace using regenerative burners, Appl. Therm. Eng. 26 (2006) 2027–2034.
[9] J. Adolfi, M. Boss, S. Santos, Commissioning Report HEC–EEC Furnace and Burners (Part 2 of 2). Tech. Rep. C108/y/2. IFRF Research Station, 2004.
[10] D. Lupant, B. Pesenti, P. Evrard, P. Lybaert, Numerical and experimental characterization of a self-regenerative flameless oxidation burner operation in a pilot-scale furnace, Combust. Sci. Technol. 179 (2007) 437–453.
[11] C. Zhang, T. Ishii, Y. Hino, S. Sugiyama, The numerical and experimental study of non-premixed combustion flames in regenerative furnaces, J. Heat Transfer 122 (2000) 287–293.
[12] W. Yang, W. Blasiak, CFD as applied to high temperature air combustion in industrial furnaces, IFRF Combust. J. (2006) 200603.
[13] W. Yang, M. Mörtberg, W. Blasiak, Influence of flame configurations on flame properties and NO emissions in combustion with high-temperature air, Scand. J. Metall. 34 (2005) 7–15.
[14] B. Danon, A. Swiderski, W. de Jong, W. Yang, D. Roekaerts, Emission and efficiency comparison of different firing modes in a furnace with four HiTAC burners, Combust. Sci. Technol. 183 (7) (2011b) 686–703.
[15] R. Hekkens, M. Mancini, Non-isothermal CFD Model of the HEC Burner and Furnace. Tech. Rep. G108/y/2. IFRF Research Station, 2004.
[16] R. Hekkens, Non-isothermal CFD Model of the HEC Burner and Furnace (Additional Calculation). Tech. Rep. G108/y/3. IFRF Research Station, 2004.
[17] D. Lupant, B. Pesenti, P. Evrard, P. Lybaert, Numerical and experimental characterization of a self-regenerative flameless oxidation burner operation in a pilot-scale furnace. In: Proceedings of the 6th High Temperature Air and Gasification Conference (HTACG). Essen, Germany; 2005.
[18] D. Lupant, B. Pesenti, P. Lybaert, Assessment of combustion models of a self-regenerative flameless oxidation burner Mons, Belgium. in: P. Lybaert (Ed.), Ninetheenth Journees d'etudes of the Belgian Section of the Combustion Institute (2006).
[19] T. Ishii, C. Zhang, S. Sugiyama, Numerical simulations of highly preheated air combustion in an industrial furnace, J. Energy Res. Technol. 120 (1998) 276–284.
[20] T. Ishii, C. Zhang, Y. Hino, Numerical study of the performance of a regenerative furnace, Heat Transfer Eng. 23 (2002) 23–33.
[21] N. Stockwell, C. Zhang, T. Ishii, Y. Hino, Numerical simulations of turbulent non-premixed combustion in a regenerative furnace, ISIJ Int. 41 (10) (2001) 1272–1281.
[22] E.S. Cho, B. Danon, W. de Jong, D. Roekaerts, Behavior of a 300 kwth regenerative multi-burner flameless oxidation furnace. Appl. Energy (in press) 2011;doi10.1016/j.apenergy.2011.06.039.
[23] Fluent 6.3 User's Guide. Fluent, Lebanon – New Hampshire, 2006.
[24] T.H. Shih, W. Liou, A. Shabbir, Z. Yang, J. Zhu, A new k–ε eddy viscosity model for high Reynolds number turbulent flows, Comput. Fluids 24 (1995) 227–238.
[25] M. Smooke, I. Puri, K. Seshadri, A comparison between numerical calculations and experimental measurements of the structure of a counterflow diffusion flame burning diluted methane in diluted air, in: Proceedings of the Twenty-First Symposium (International) on Combustion, 21, 1986, pp. 1783–1792.
[26] Physical Properties of Natural Gases. Nederlandse Gasunie N.V., 1980.
[27] I. Ertesvåg, B. Magnussen, The eddy dissipation turbulence energy cascade model, Combust. Sci. Technol. 159 (2000) 213–235.
[28] F. Christo, B. Dally, Modeling turbulent reacting jets issuing into a hot and diluted coflow, Combust. Flame 142 (2005) 117–129.
[29] J.P. Kim, U. Schnell, G. Scheffknecht, A. Benim, Numerical modelling of mild combustion for coal, Prog. Comput. Fluid Dyn. 7 (2007) 337–346.
[30] A. Parente, C. Galletti, L. Tognotti, Effect of the combustion model and kinetic mechanism on the MILD combustion in an industrial burner fed with hydrogen enriched fuels, Int. J. Hydrogen Energy 33 (2008) 7553–7564.
[31] G. Stefanidis, B. Merci, G. Heynderickx, G. Marin, CFD simulations of steam cracking furnaces using detailed combustion mechanisms, Comput. Chem. Eng. 30 (2006) 635–649.
[32] J. Kim, U. Schnell, G. Scheffknecht, Comparison of different global reaction mechanisms for mild combustion of natural gas, Combust. Sci. Technol. 180 (2008) 565–592.
[33] S. Pope, Computationally efficient implementation of combustion chemistry using in situ adaptive tabulation, Combust. Theor. Model. 1 (1997) 41–63.
[34] B. Danon, W. de Jong, D. Roekaerts, Experimental and numerical investigation of a flox combustor firing low calorific value gases, Combust. Sci. Technol. 182 (9) (2010) 1261–1278.
[35] A. De, E. Oldenhof, P. Sathiah, D. Roekaerts, Numerical simulation of Delft-Jet-in-Hot-Coflow (DJHC) flames using the Eddy Dissipation Concept model for turbulence-chemistry interaction. Flow Turbul. Combust. (in press) 2011; doi10.1007/s10494-011-9337-0.
[36] R. Gordon, A. Masri, S. Pope, G. Goldin, Transport budgets in turbulent lifted flames of methane autoignition in a vitiated co-flow, Combust. Flame 151 (2007) 495–511.
[37] R. Bilger, S. Stårner, R. Kee, On reduced mechanisms for methane-air combustion in nonpremixed flames, Combust. Flame 80 (1990) 135–149.
[38] E. Grandmaison, I. Yimer, H. Becker, A. Sobiesiak, The strong-jet/weak-jet problem and aerodynamic modeling of the CGRI burner, Combust. Flame 114 (1998) 381–396.